Proton Conduction in Dense and Porous Nanocrystalline Ceria Thin Films

Giuliano Gregori, Mona Shirpour, and Joachim Maier*

The electrical conductivity of ceria thin films (epitaxial as well as dense and porous nanocrystalline) is investigated in dry and wet atmosphere at temperatures below 500 °C. For the epitaxial and the fully dense nanocrystalline samples, no significant differences can be observed between dry and wet conditions. In marked contrast, the nanocrystalline porous films obtained via spin coating exhibit a considerable enhancement of the protonic conductivity below 300 °C in wet atmosphere. This outcome reveals that the residual open mesoporosity plays the key role for the enhancement of the proton transport at low temperatures and not the high density of grain boundaries. The quantitative analysis of the various pathways, along which the proton transport can take place, indicates that the observed proton conduction can arise not only from bulk water adsorbed in the open pores but also from the space charge zones on the water side of the water/oxide interface.

1. Introduction

Although oxides with a fluorite structure such as zirconia and ceria are known to be rather poor proton conductors,[1] a number of different nanocrystalline compounds, for example, yttrium-doped zirconia (YSZ),[2–5] samarium-doped ceria (SDC)[2–4,6] as well as gadolinium-doped ceria (GDC)[7–10] have gained much attention because of enhanced proton conductivity at temperatures below 200 °C. Similar effects were recently observed also in nanocrystalline TiO_2.[11] Albeit a number of independent contributions have reported on this phenomenon, the origin of such peculiar behavior is still controversial and matter of investigations, the main open question being whether the enhanced proton conduction occurs along the grain boundaries[2–4,8,12] or rather along residual pores and cracks still present in the material.[5,7,9,10,13] According to the first hypothesis, protons should migrate along the core of the grain boundaries as the space charge zones appear to be rather blocking.[3] The second explanation takes into account the residual porosity, which is naturally present in most nanocrystalline ceramics due to the low sintering temperature, and that can allow water adsorption in wet conditions.[5,9,13] In this case, the adsorbed water is responsible for the enhanced proton conduction at low temperatures (cf. also the discussion). In line with this, the proton conduction of dense nanocrystalline YSZ ceramics could be recently observed only at 50 °C and was limited to the sample surface.[14] It is also worth noting that there is a vast literature reporting on the proton conduction of porous oxides,[15,16] and studies showing enhanced proton conduction in oxide powders[17] at low temperatures.

Interestingly, as far as ceria is concerned, recent investigations[18] aimed at determining whether the grain size can affect the enthalpy of water adsorption ΔH_{ad} revealed that the value of ΔH_{ad} remains essentially constant between nanocrystalline and microcrystalline undoped CeO_2 powders (–59.8 vs –61.7 kJ mol^{-1} for the same water coverage). Such values of ΔH_{ad} point towards chemisorption rather than physisorption as main adsorption mechanism on ceria, and seem to indicate that the higher concentration of oxygen vacancies on the surface of nanocrystalline ceria[19,20] does not influence ΔH_{ad}.

In this study, we compare the electrical conduction properties (measured via impedance spectroscopy) of fully dense epitaxial and nanocrystalline ceria thin films (undoped as well as 10 mol% Gd-doped 10GDC) grown via pulsed-laser deposition (PLD) with those of porous nanocrystalline films prepared by spin coating (SC) with the purpose of inspecting the role of the residual porosity with regard to the enhanced low temperature conductivity (θ <300 °C). It is worth noting here that, as shown below, the nanocrystalline dense PLD films and nanocrystalline porous SC films considered in this study exhibit comparable average grain size.

The proton conduction in dense nanocrystalline zirconia PLD films was already addressed previously;[21] however, at too high temperatures (θ >500 °C) as to detect this proton transport phenomena occurring at low temperatures. Nonetheless, evidences of proton conductivity in nanocrystalline atomic-layer-deposited YSZ (film thickness 200 nm and grain size 20–30 nm)[22] and porous YSZ films were recently reported.[23]

2. Results and Discussion

Figure 1 summarizes the X-ray diffraction (XRD) patterns collected from the different films investigated in the present study. The PLD films (Figure 1a) deposited on SiO_2 exhibit, as

G. Gregori, M. Shirpour,[+] Prof. J. Maier
Max Planck Institute for Solid State Research
Heisenbergstr. 1, D-70569 Stuttgart, Germany
E-mail: g.gregori@fkf.mpg.de
[+] Present address: Environmental Energy Technologies Division, Lawrence Berkeley National Laboratory, One Cyclotron Road, Berkeley, CA 94720, USA

DOI: 10.1002/adfm.201300527

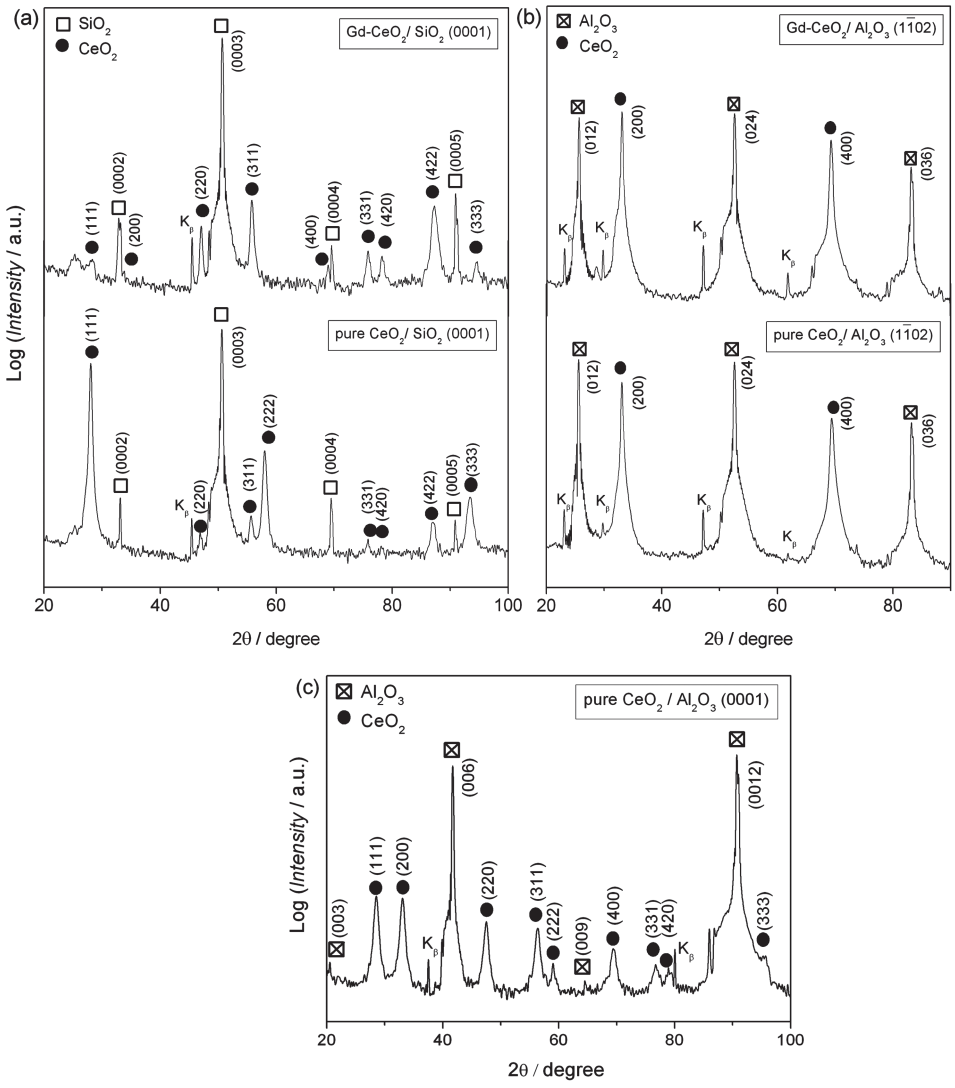

Figure 1. XRD patterns acquired from a) the PLD films grown on SiO_2, b) PLD films grown on Al_2O_3, and c) spin coated films.

expected, a polycrystalline microstructure, those grown on Al_2O_3 are epitaxial (Figure 1b), while the spin-coated films (Figure 1c) are polycrystalline. Transmission electron microscopy (TEM) analysis performed on the cross sections of some representative samples reveals that the polycrystalline PLD films (**Figure 2**a) are fully dense, whereas the SC films (Figure 2b) are characterized by the presence of nanosized residual porosity with a pore size on the order of 5–10 nm.

Note also that the average grain size of the SC samples (20 nm) is comparable to the average lateral grain size of the polycrystalline PLD thin films.

All impedance spectra collected from the samples considered here consist of a single semicircle when plotted in the Nyquist diagram ($-Z_{imag}$ vs Z_{real}). This is due to a stray capacitance of about 1.5 pF, which makes it impossible to distinguish between bulk and grain boundary contributions of these polycrystalline samples.

Figure 3 illustrates the conductivity data collected from all the PLD samples: the circles refer to the measurements carried out in dry atmosphere, while the triangles correspond to wet conditions (water partial pressure pH_2O =20 mbar). In dry and low oxygen partial pressure (N_2 grade 5.0) conditions, one expects predominantly electronic conductivity in the epitaxial and nanocrystalline undoped CeO_2 thin films. Figure 3a shows that the conductivity σ of the nanocrystalline undoped film decreases from 500 to 200 °C with an activation energy of 1.08 eV, which is consistent with previous measurements carried out on similar samples.[38] Below 250 °C, the overall impedance of the thin films is so high (10^{10}–10^{11} Ω) that it is impossible to properly fit the experimental spectra and obtain reliable data. The only slight difference of conductivity values between wet (σ_{wet}) and dry conditions (σ_{dry}) together with the activation energy values (1.08 eV in both wet and dry atmosphere) indicate that the conduction mechanism does not change when the samples are exposed to the humidified gas.

The only difference is that, below 50 °C, the conductivity sharply increases in wet atmosphere. The epitaxial undoped thin film (Figure 3b) exhibits a very similar behavior (in both

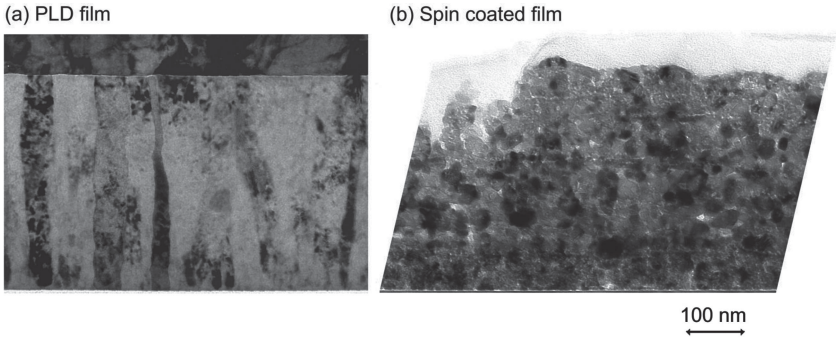

Figure 2. TEM images illustrating the microstructure of a) a PLD film grown on SiO_2[38] (reproduced with permission of the PCCP Owner Societies) and b) a spin coated film deposited on Al_2O_3. In the latter, the residual mesoscopic porosity can be clearly recognized.

dry and wet conditions) compared with the nanocrystalline film of the same composition. Also the activation energy value is very close to the one of the first sample and this is consistent with previous investigations.[38] It is important to emphasize here that both the epitaxial and the (fully dense) nanocrystalline PLD films do not exhibit any perceptible difference between dry and wet conditions. This is consistent with previous findings showing that the solubility of protons in the bulk of ceramic CeO_2 is rather low.[24]

The low temperature (θ <50 °C) enhancement of the conductivity observed in both samples is most probably related to water adsorption occurring at the top surface of the films. A similar conductivity enhancement below 50 °C was also observed for nanocrystalline YSZ films.[25]

Figure 3c,d show the Arrhenius diagrams for the polycrystalline and the epitaxial 10GDC films (PLD), respectively. Under dry conditions, both the activation energy (0.7 eV) and the high conductivity values indicate, as expected,

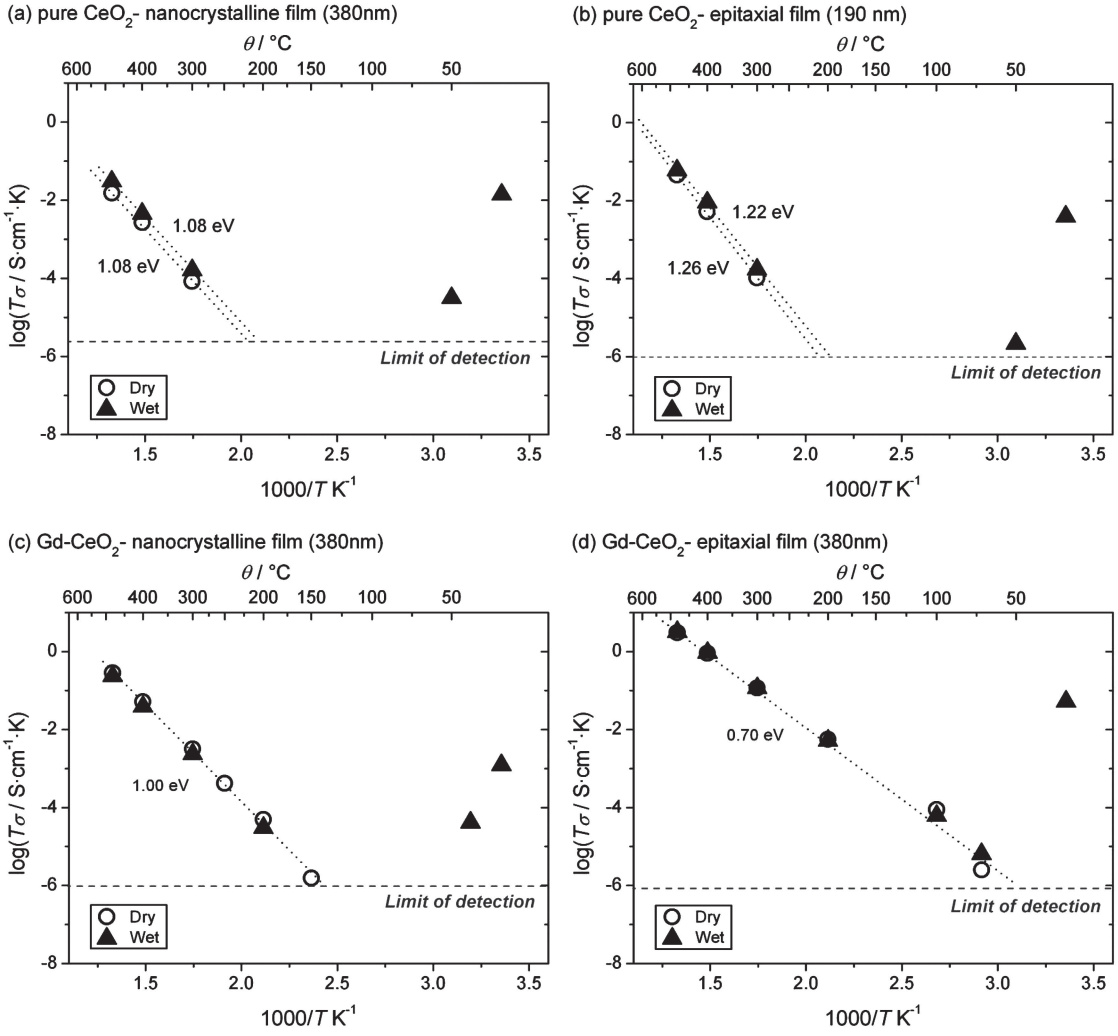

Figure 3. Conductivity of the dense PLD films a) nanocrystalline pure ceria, b) epitaxial pure ceria, c) nanocrystalline Gd-doped ceria, and d) epitaxial Gd-doped ceria under dry (circles) and wet (triangles) conditions. Notably, for all samples, there is no change of the measured conductivity between dry and wet conditions except for the measurements carried out in wet atmosphere and low temperatures ($\theta \leq 50$ °C).

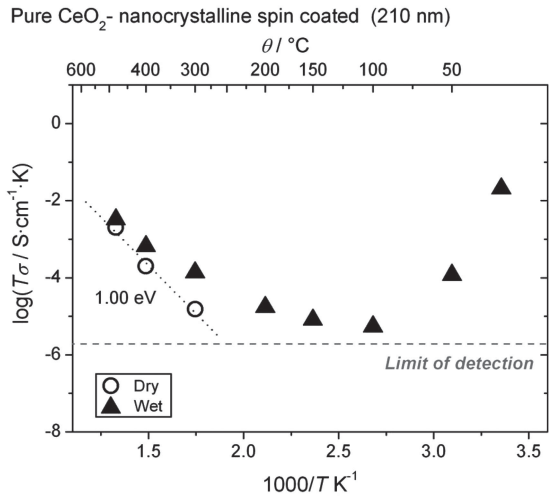

Figure 4. Conductivity of a porous pure ceria thin film under dry and wet conditions. Already at 300 °C the conductivity measured under wet conditions (triangles) is significantly higher than the one collected in dry atmosphere (circles).

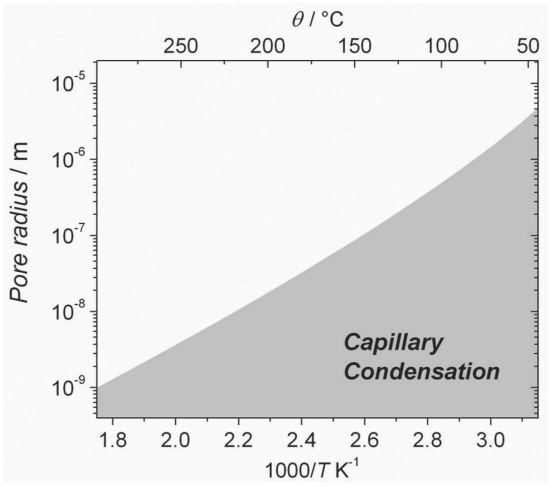

Figure 5. Pore radius at which water condensation due to capillary effects occurs (gray area) as calculated according to Equation 1 assuming γ and V_m to be temperature independent.

oxygen vacancy migration in the sample. The polycrystalline film exhibits i) higher activation energy and ii) lower conductivity in agreement with a recent study on nanocrystalline thin films.[38] Remarkably, also in these cases, above 50 °C, the data acquired under dry conditions and those collected in humidified atmosphere only slightly differ from each other (while exhibiting the same activation energy), indicating that at those temperatures the dominating conduction mechanism is the same (namely oxygen vacancy migration) under wet as well as dry conditions. Similar to the undoped CeO_2 films, the enhanced conductivity below 50 °C is most likely due to the condensation of water on the top surface.

Figure 4 summarizes the conductivity data determined for the spin coated undoped CeO_2 thin films with a thickness of 200 nm. Under dry conditions, this sample exhibits conductivity and activation energy values, which are very similar to those of the PLD films (in dry atmosphere) and are characteristic of electronic conduction in nanocrystalline ceria thin films.[38] Under wet conditions, the porous film shows a significant conductivity enhancement (one order of magnitude) already at 300 °C. The difference between σ_{wet} and σ_{dry} becomes much more pronounced at lower temperatures.

It is worth noting that the behavior at θ <300 °C is consistent with a previous study, showing that the enhanced protonic conductivity in nanocrystalline ceramics occurs in presence of residual mesoporosity and in concomitance with a considerable water uptake.[9] Water adsorption in nanocrystalline ceramics was recently confirmed by other independent studies.[5,13] This is consistent also with capillary condensation effects occurring at the nanoscale, which can be rationalized by taking into account the Kelvin equation:[26]

$$\frac{1}{r} = \frac{RT}{\gamma V_m} \ln\left(\frac{p_{vap}}{p_{sat}}\right) \quad (1)$$

where, r is the radius of curvature of the liquid-gas interface, R is gas constant, T the temperature (in Kelvin), γ the surface tension (for water, we take here γ =0.07 J m^{-2}), V_m the molar volume,[27] p_{vap} the vapour pressure, and p_{sat} the saturation pressure. Since, according to our experimental set-up, p_{vap} = 20 mbar and as p_{sat} can be obtained from the existing literature,[28] we can estimate for each temperature the maximum size of the pores at which water capillary condensation is likely to occur. According to this calculation, residual open pores with a diameter of ≈5 nm allow water condensation already at 250 °C as shown in **Figure 5**.

In order to explain the enhanced conductivity at θ <300 °C, we consider here 4 possible transport pathways, which are schematically depicted in **Figure 6**. As both epitaxial films (undoped as well as 10GCO) do not exhibit any enhanced conductivity in wet conditions, we can rule out bulk transport (pathway 1) to be the main mechanism behind the enhanced conduction at low temperatures.

Also the grain boundary pathways (case 2 in Figure 6) can be excluded since no improvements of the conductivity can be observed for the polycrystalline PLD samples (which are fully dense) when changing from dry to wet atmosphere.

In light of these considerations, and taking into account that the average lateral grain size of the polycrystalline PLD films is comparable to the average grain size of the spin coated films, we conclude that the residual porosity is responsible for the enhanced proton conduction at low temperatures (θ <300 °C) and not the high density of grain boundaries. As pointed out above, this is consistent with previous thermogravimetric (TG) analysis showing a significant water uptake below 200 °C in porous nanocrystalline ceria ceramics.[5,9,13]

Hence, we can assume that the conduction occurs along the surface of the pores. The question that remains open is whether the conduction occurs predominantly within the water layer adsorbed on the surface of the pores (pathway 3) or, alternatively, since protons can even be injected into the material, in the solid space charge zone right below the surface (pathway 4). Here, it is important to note that due to thermodynamic reasons space charge effects are always present at interfaces and thus need to be considered. Obviously, the key aspect is

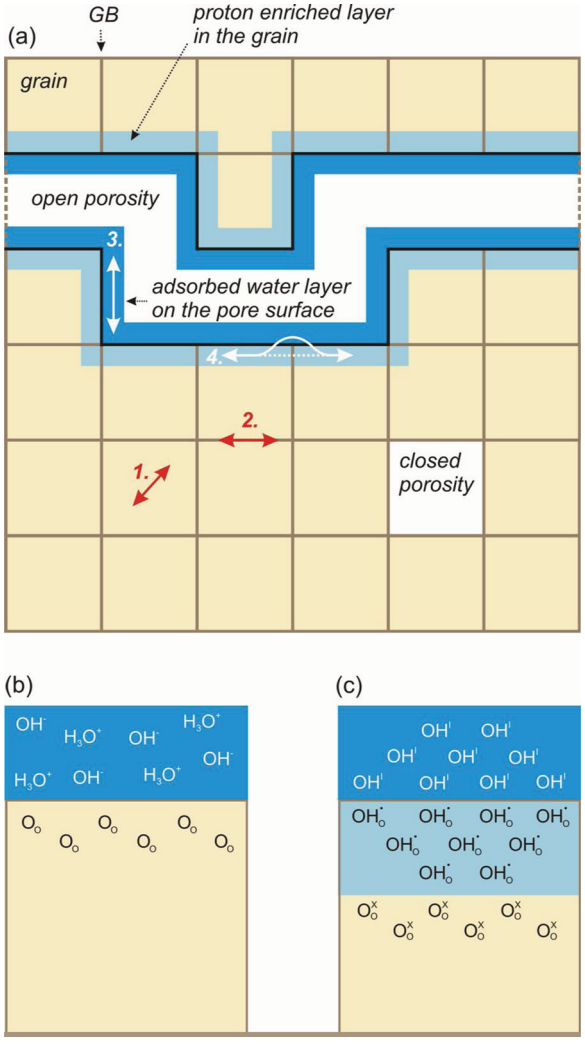

Figure 6. a) Schematic 2D representation of the microstructure of the porous nanocrystalline films. Four proton transport pathways are considered: 1 transport in the bulk, 2 along the GBs, 3 on the open pores surfaces in the adsorbed water layer, and 4 in a proton enriched layer right below the pore/oxide interface. b) Detail of pathway 3, in which protons dissociate according to Equation 2 and migrate according to Equation 3. c) Detail of pathway 4 represented in the Kröger-Vink notation: in this case protons (H^+) get injected into CeO_2 according to Equation 4 and migrate according to Equation 5. In (b) and (c) the neutral water molecules as well as the neutral Ce and O lattice sites in ceria are not shown. It is also worth noting that in case (b) space charge effects may be present with their contribution being however negligible while in case (c) bulk water conduction is present but negligible with respect to space charge effects.

whether such effects are relevant, namely, whether they can induce significant enhancement of the mobile charge carrier concentrations resulting in the measured conductivity or not.

In the former case, the dissociation equilibrium (constant K_w) defines the proton and the hydroxide concentration in the water layer according to (see also Figure 6b):

$$H_2O(l) + H_2O(l) \rightleftharpoons H_3O^+(l) + OH^-(l), \quad (2)$$

(l indicates here the liquid phase) and the transport reaction can be written as

$$H_3O^+(l, x) + H_2O(l, x') \rightleftharpoons H_2O(l, x) + H_3O^+(l, x'), \text{ or}$$
$$H_2O(l, x) + OH^-(l, x') \rightleftharpoons OH^-(l, x) + H_2O(l, x') \quad (3)$$

with x and x' indicating different positions. Note that here we assume the water layer to be neutral. Thus, since the mobility of protons is larger (yet with the same order of magnitude) than the mobility of the hydroxide, H_3O^+ are expected to be the main charge carriers.[29] In the latter situation (pathway 4), the proton (H^+) insertion in the oxide reads as[30]

$$H_2O(l) \rightleftharpoons OH^-(l) + H^+(s) \quad (4a)$$

(s indicates here the solid) or more properly in the Kröger-Vink notation (see Figure 6c)

$$H_2O(l) + O_O^X(s) \rightleftharpoons OH^{/}(l) + OH_O^{\bullet}(s) \quad (4b)$$

The corresponding migration reaction is then

$$OH_O^{\bullet}(x) + O_O^X(x') \rightleftharpoons O_O^X(x) + OH_O^{\bullet}(x') \quad (5)$$

Let us now consider pathway 3, according to which the proton transport occurs along the water layer adsorbed on the walls of the open pores (Figure 6b and Equation 3). As shown in the literature,[31] in such a configuration, and according to the brick layer model, the measured conductivity σ_m can be expressed as

$$\sigma_m = \beta \varphi_P \Omega a \sigma_{\infty,L} \quad (6)$$

where ϕ_P is the open porosity volume fraction. According to the brick layer model, $\beta = 2/3$,[32] Ω, which is the surface-to-volume fraction of a pore, is equal to $6/d$ (d being the average pore size), a is the thickness of the adsorbed water layer, and $\sigma_{\infty,L}$ is the bulk proton conductivity within the water layer. Equation 6 can be simplified as

$$\sigma_m = \frac{4a}{d} \varphi_P \sigma_{\infty,L}. \quad (7)$$

Figure 7 shows the dependence of $\sigma_{\infty,L}/\sigma_m$ on a set of realistic values of d/a (here ranging between 10 and 100) and ϕ_P (spanning between 0.05 and 0.3) for θ = 200 °C (σ_m =3.35 × 10^{-8} S cm^{-1}). From these, it is possible to estimate the proton mobility within the water layer to range between 8×10^{-2} and 6×10^{-4} $cm^2 V^{-1} s^{-1}$).[33,34] These values are comparable

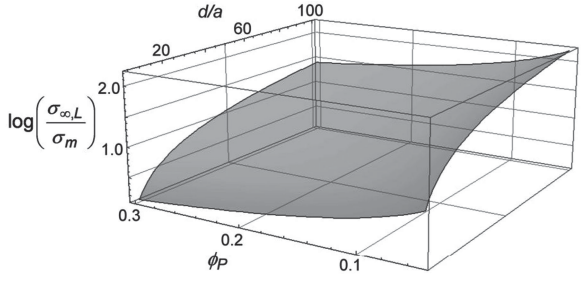

Figure 7. Pathway 3: normalized conductivity $\sigma_{\infty,L}/\sigma_m$ (Equation 7) as a function of i) the ratio between the average pore size d and the water layer thickness a and ii) the open porosity volume fraction ϕ_P.

with what was previously reported in the literature,[35] for the self diffusion of H_3O^+ in water ($u_{self} \approx 8 \times 10^{-3}$ cm^2 V^{-1} s^{-1} at 200 °C).[36]

This indicates that proton conduction within the water layer adsorbed on the walls of the open porosity is absolutely plausible (pathway 3). It is important to emphasize that the proton transport mechanism considered so far is proton conduction in "bulk" water under the assumption that the possibly present space charge effects are negligible. If, however, such effects are perceptible, then the measured proton conductivity can arise from an enhanced charge carrier concentration at the water/oxide interface.

Let us now discuss such a possibility by considering the fourth and last case, namely the situation in which, upon dissociation in the neutral water layer adsorbed in the pore, protons (H^+) get injected into CeO_2 and move along pathways parallel to the surface (Figure 6).

Also in this case, we can adopt the same geometrical model used for the pathway 3 (Equation 6). Note that for this situation, the bulk conductivity is negligible and thus one can write:[31]

$$\sigma_m = \beta \varphi_P \left(\frac{2\lambda}{d_P}\right) \sigma_S \quad (8)$$

with $\beta = 2/3$ and d_P being the average size of the open pores. For the proton concentration, we can assume a Gouy-Chapman profile, according to which λ, the Debye length, $\sigma_S = e\, u_S \sqrt{c_0 c_\infty}$ is the proton conductivity in the solid arising from the layer right below the water/oxide interface, where u_S is the proton mobility in CeO_2. Thus, Equation 7 now becomes

$$\sigma_m = \frac{2}{3}\varphi_P \frac{12\lambda}{d_P} e\, u_S \sqrt{c_0 c_\infty} = 8\varphi_P \frac{1}{d_P} u_S \sqrt{\varepsilon_0 \varepsilon_r k T c_0} \quad (9)$$

Note that according to the Gouy-Chapman model, c_0 is the proton concentration in the very first layer of CeO_2, right below the water/oxide interface.

By considering Equation 9, we estimate which range of u_S, c_0, d, and ϕ_P can yield the measured conductivity σ_m (as in the previous case, we consider here $\sigma_m = 3.35 \times 10^{-8}$ S cm^{-1} taken at 200 °C). **Figure 8** illustrate the case for $\phi_P = 0.2$ (which lies in the middle of the range considered in Figure 7).

As c_0 must be lower than the concentration of oxygen anions in CeO_2 ($\log([O^X_O]$ cm$^{-3}) = 22.7$), a reasonable range of u_S within which the measured conductivity might be due to proton injected in ceria lies above $\log(u_S/\text{cm}^2\,\text{V}^{-1}\,\text{s}^{-1}) = -9.15$, that is, $u_S = 7 \times 10^{-10}$ cm^2 V^{-1} s^{-1}. This is a reasonable value since the mobility of protons in 10% yttrium-doped barium zirconate (one of the best oxide proton conductors) is equal to 3×10^{-6} cm^2 V^{-1} s^{-1} (at 200 °C).[37]

Nonetheless, it is worth noting that an increase of the proton concentration on the ceria side of the water/oxide interface would be counterbalanced by an enhancement of the hydroxide concentration in the water layer (space charge layer) in proximity of the interface, which, thanks to the higher mobility of hydroxide in water, would even exceed the conductivity of protons in ceria. Therefore, space charge effects on the water side of the water/oxide interface can fully explain the occurrence of proton conduction at low temperatures.

In this context, it must be also noticed that the occurrence of such effects (redistribution of the charge carrier concentrations in proximity of the water/oxide interface) depends on a set of additional parameters such as the actual pH value of the water layer and the point of zero charge of nanocrystalline ceria. Further tests are currently in progress in order to address these aspects.

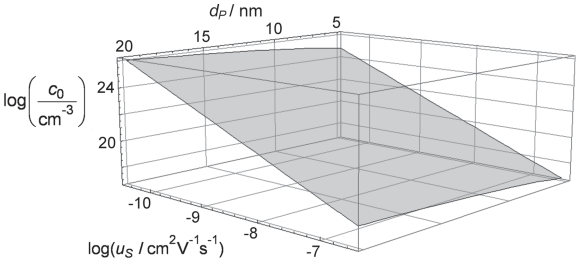

Figure 8. Pathway 4: concentration of the protons right below the water/ceria interface, $\log(c_0)$, calculated according to Equation 9 as function of the open pores average size d_P and the proton mobility in ceria u_S.

3. Conclusions

We have compared the electrical conduction properties (under both dry and wet conditions) of a number of different samples, namely dense epitaxial and nanocrystalline (grown via pulsed laser deposition) as well as porous spin coated films.

Remarkably, despite the large grain boundary volume fraction, the fully dense nanocrystalline films do not exhibit any conductivity enhancement in wet atmosphere. The conductivity increase observed only at 50 °C is a common feature of all samples and is ascribed to the adsorption of water on the top surface of the films.

In contrast, the porous nanocrystalline thin films show a perceptible conductivity within a temperature range, in which the dense PLD films display such low conductance that it is not possible to record reliable impedance spectra.

This different behavior between porous and dense nanocrystalline films in wet conditions points towards the residual open porosity to be the key factor for the protonic conductivity at low temperatures, rather than the large density of grain boundaries. In particular, the analysis of the experimental data indicates that the proton transport takes place within the water layer: the aspect that still needs to be addressed is whether the conduction occurs in "bulk" water or in the space charge layer on the water side of the water/oxide interface.

4. Experimental Section

Thin Films Fabrication: Here, nominally pure ceria (CeO_2) as well as 10 mol% Gd-doped CeO_2 (10GDC) thin films were fabricated via PLD as described elsewhere.[38] Different substrates (10 mm × 10 mm × 0.5 mm) were employed to obtain nanocrystalline (on SiO_2 (0001)) and epitaxial (on Al_2O_3 ($1\bar{1}02$)) microstructures, respectively. The thickness of the various films ranged between 200 and 400 nm. Porous nanocrystalline films of undoped CeO_2 were prepared by SC as described elsewhere,[39,40] starting from a solution of cerium nitrate ($Ce(NO_3)_3{\cdot}6H_2O$, Sigma Aldrich 99.99%) (0.02 mol was dissolved in 10 mL bi-distilled water), 40 mL ethylene glycol, and 10 mL of nitric acid (10 M). The solution was spun on sapphire substrates (0001) (CrysTec GmbH) using a SCE spin

coater (3400 rpm for 30 s). After each deposition, the sample was pre-baked at 80 °C for one minute on a hot plate and then baked at 300 °C on a preheated hot plate for another minute. Upon cooling down to room temperature, this procedure was repeated 10 times, in order to obtain the desired thickness. Finally, the film was annealed at 600 °C for one hour (heating rate 5 °C min^{-1}, cooling rate 3 °C min^{-1}) in air.

Microstructure Characterization: X-ray diffraction analysis was performed using a Philips Xpert XRD diffractometer (3710 HTK, Cu K_α = 1.5418 Å), while transmission electron microscopy was carried using a Zeiss 912 Omega TEM microscope with an acceleration voltage of 200 kV.

Electrical Conductivity Measurements: Upon deposition of two parallel platinum electrodes with a size of 4.5 mm × 10 mm each and a thickness of about 400 nm (Edwards Auto 306 sputtering system) the electrical conductivity measurements under dry and wet conditions (water partial pressure, pH_2O = 20 mbar) were performed by means of a Novocontrol Alpha-A impedance spectrometer (a.c. voltage amplitude 0.1 V, frequency range 1 MHz–1 Hz). The humidified conditions were obtained by passing the carrier gas (nitrogen grade 5.0) through a water bubbler which was kept at the constant temperature of 17 °C, which corresponds to a water partial pressure pH_2O of 20 mbar. For the dry conditions, the traces of water possibly present in nitrogen 5.0 were condensed by passing the gas through a cold trap (dry ice) before entering the measurement cell. The residual oxygen partial pressure of nitrogen 5.0 was checked with a commercial oxygen sensor (Rapidox 2100, Cambridge Sensotec) and amounted 10^{-5}–10^{-6} atm.

In order to be sure that the samples were at equilibrium with the surroundings, conductivity relaxation was examined upon the change of the experimental conditions.

Acknowledgements

The authors wish to thank M. C. Göbel (MPI for Solid State Research, Stuttgart) for the preparation of the PLD films, M. Kelsch (MPI for Intelligent Systems, Stuttgart) for the TEM sample preparation, and K. Hahn as well as P. Kobold (MPI for Intelligent Systems, Stuttgart) for the TEM analysis.

Received: February 8, 2013
Revised: April 5, 2013
Published online: June 20, 2013

[1] C. Wagner, *Ber. Bunsenges. Phys. Chem.* **1968**, *72*, 778.
[2] S. Kim, U. Anselmi-Tamburini, H. J. Park, M. Martin, Z. A. Munir, *Adv. Mater.* **2008**, *20*, 556.
[3] S. Kim, H. J. Avila-Paredes, S. Z. Wang, C. T. Chen, R. A. De Souza, M. Martin, Z. A. Munir, *Phys. Chem. Chem. Phys.* **2009**, *11*, 3035.
[4] G. Chiodelli, F. Maglia, U. Anselmi-Tamburini, Z. A. Munir, *Solid State Ionics* **2009**, *180*, 297.
[5] S. Miyoshi, Y. Akao, N. Kuwata, J. Kawamura, Y. Oyama, T. Yagi, S. Yamaguchi, *Solis State Ionics* **2012**, *207*, 21.
[6] H. Takamura, N. Takahashi, *Solid State Ionics* **2010**, *181*, 100.
[7] E. Ruiz-Trejo, J. A. Kilner, *J. Appl. Electrochem.* **2009**, *39*, 523.
[8] H. J. Avila-Paredes, J. F. Zhao, S. Z. Wang, M. Pietrowski, R. A. De Souza, A. Reinholdt, Z. A. Munir, M. Martin, S. Kim, *J. Mater. Chem.* **2010**, *20*, 990.
[9] M. Shirpour, G. Gregori, R. Merkle, J. Maier, *Phys. Chem. Chem. Phys.* **2011**, *13*, 937.
[10] D. Perez-Coll, E. Sanchez-Lopez, G. C. Mather, *Solid State Ionics* **2010**, *181*, 1033.
[11] F. Maglia, I. G. Tredici, G. Spinolo, U. Anselmi-Tamburini, *J. Mater. Res.* **2012**, *27*, 1975.
[12] R. A. De Souza, Z. A. Munir, S. Kim, M. Martin, *Solid State Ionics* **2011**, *196*, 1.
[13] M. J. Pietrowski, R. A. De Souza, S. Kim, Z. A. Munir, M. Martin, *Solid State Ionics* **2012**, *225*, 241.
[14] C. Tandé, D. Pérez-Coll, G. C. Mather, *J. Mater. Chem.* **2012**, *22*, 11208.
[15] M. Nogami, R. Nagao, C. Wong, *J. Phys. Chem. B* **1998**, *102*, 5772.
[16] M. T. Colomer, *J. Eur. Ceram. Soc.* **2006**, *26*, 1231.
[17] S. Raz, K. Sasaki, J. Maier, I. Riess, *Solid State Ionics* **2001**, *143*, 181.
[18] S. Hayun, S. V. Ushakov, A. Navrotsky, *J. Am. Ceram. Soc.* **2011**, *94*, 3679.
[19] A. Kossoy, Y. Feldmann, E. Wachtel, K. Gartsman, I. Lubomirsky, J. Fleig, J. Maier, *Phys. Chem. Chem. Phys.* **2006**, *8*, 1111.
[20] S. Deshpande, S. Patil, S. V. N. T. Kuchibhatla, S. Seal, *Appl. Phys. Lett.* **2005**, *87*, 133113.
[21] X. Guo, E. Vasco, S. Mi, K. Szot, E. Wachsman, R. Waser, *Acta Mater.* **2005**, *53*, 5161.
[22] J. S. Park, Y. B. Kim, J. H. Shim, S. Kang, T. M. Gur, F. B. Prinz, *Chem. Mater.* **2010**, *22*, 5366.
[23] B. Scherrer, M. V. F. Schlupp, D. Stender, J. Martynczuk, J. G. Grolig, H. Ma, P. Kocher, T. Lippert, M. Prestat, L. J. Gauckler, *Adv. Funct. Mater.* **2013**, *23*, 1957.
[24] N. Sakaia, K. Yamajia, T. Horita, H. Yokokawa, Y. Hirata, S. Sameshima, Y. Nigara, J. Mizusaki, *Solid State Ionics* **1999**, *125*, 325.
[25] H. J. Avila-Paredes, E. Barrera-Calva, H. U. Anderson, R. A. De Souza, M. Martin, Z. A. Munir, S. Kim, *J. Mater. Chem.* **2010**, *20*, 6235.
[26] W. Thomson, *Proc. R. Soc. Edinburgh* **1870**, *7*, 63.
[27] The molar volume can be determined in first approximation using the ideal gas law.
[28] F. W. Murray, *J. Appl. Meteor.* **1967**, *6*, 203.
[29] P. W. Atkins, *Physical Chemistry, 6th ed.*, Oxford University Press, Oxford, UK **2000**, Ch. 24.
[30] It is worth noting that due to electrostatic interactions, one would expect the positively charged H^+ to approach the O^{2-} anions of CeO_2 (cf. Equation 4b).
[31] J. Maier, *Prog. Solid State Chem.* **1995**, *23*, 171.
[32] We assume here for simplicity that the open porosity is percolating.
[33] The proton concentration in pure neutral water is $[H_3O^+] = 6 \times 10^{13}$ cm^{-3}. However one should notice that with increasing temperature (at least up to 300 °C) K_w significantly increases. If one takes $K_w = 10^{-11.5}$ (θ = 200 °C), then $[H_3O^+] = 1 \times 10^{15}$ cm^{-3} which implies that (for the range of d/a ϕ_P and considered here) the proton mobility spans from 8×10^{-2} to 6×10^{-4} cm^2 V^{-1} s^{-1}.
[34] R. E. Mesmer, W. L. Marshall, D. A. Palmer, J. M. Simonson, H. F. Holmes, *J. Sol. Chem.* **1988**, *17*, 699.
[35] K. D. Kreuer, in *Proton Conductors: Solids Membranes, and Gels - Materials and Devices*, (Ed: P. Colomban), Cambridge University Press, Cambridge, UK **1992**.
[36] If OH^- is the mobile charge carrier, one expects mobility values of the same order of magnitude.
[37] K. D. Kreuer, *Ann. Rev. Mater. Res.* **2003**, *33*, 333.
[38] M. C. Göbel, G. Gregori, X. X. Guo, J. Maier, *Phys. Chem. Chem. Phys.* **2010**, *12*, 14351.
[39] C. C. Chen, M. M. Nasrallah, H. U. Anderson, *J. Electrochem. Soc.* **1993**, *140*, 3555.
[40] T. Suzuki, I. Kosacki, H. U. Anderson, *Solid State Ionics* **2002**, *151*, 111.